Available online at www.sciencedirect.com
ScienceDirect
Carbohydrate Research 342 (2007) 2075–2085
Carbohydrate RESEARCH

Two interconverting pentaiodide forms in the cyclomaltohexaose (α-cyclodextrin) polyiodide inclusion complex with sodium ion: dielectric and Raman spectroscopy studies

Vasileios G. Charalampopoulos and John C. Papaioannou*

Laboratory of Physical Chemistry, Department of Chemistry, National and Kapodistrian University of Athens, PO BOX 64004, 157 10 Zografou, Athens, Greece

Received 13 April 2007; received in revised form 21 May 2007; accepted 22 May 2007
Available online 2 June 2007

Abstract—The polycrystalline inclusion complex of cyclomaltohexaose, $(\alpha\text{-CD})_2{\cdot}NaI_5{\cdot}8H_2O$, has been investigated via dielectric spectroscopy over a frequency range of 0–100 kHz and the temperature range of 125–450 K. Additionally, a Raman spectroscopy study was accomplished in the temperature ranges of (i) 153–298 K and (ii) 303–413 K. The $\ln\sigma$ versus $1/T$ variation revealed the order–disorder transition of some normal hydrogen bonds to those of a flip-flop type at 200.9 K. From 278.3 up to 357.1 K, the progressive transformation $(H_2O)_{\text{tightly bound}} \rightarrow (H_2O)_{\text{easily movable}}$ takes place resulting in an Arrhenius linear increment of the ac-conductivity with activation energy $E_a = 0.32$ eV. In the range of 357.1–386.1 K a second linear part with $E_a = 0.55$ eV is observed, indicating the contribution of sodium ions via the water-net. The rapid decrease of the ac-conductivity at $T > 386.1$ K is due to the removal of the water molecules from the crystal lattice, whereas the abrupt increase at $T > 414.9$ K is caused by the sublimation of iodine. The Raman bands at 160 and 169 cm^{-1} indicate the coexistence of $(I_2{\cdot}I^-{\cdot}I_2)$ and $(I_3^-{\cdot}I_2 \leftrightarrow I_2{\cdot}I_3^-)$ units, respectively. The $(I_3^-{\cdot}I_2 \leftrightarrow I_2{\cdot}I_3^-)$ units are presented as form (I), and their central I^- ion is disordered in occupancy ratio different from 50/50 (e.g., …60/40…70/30…). The $(I_2{\cdot}I^-{\cdot}I_2)$ units are displayed by the 2 equiv forms (IIa) and (IIb). In (IIa) the central I^- ion is twofold disordered in an occupancy ratio of 50:50, whereas in (IIb) the central I^- ion is well-ordered and equidistant from the two I_2 molecules. At low temperatures the transformation (I)→(IIa) takes place, whereas at high temperatures the inverse one (IIa)→(I) happens. X-ray powder diffraction and Rietveld analysis revealed a triclinic crystal form with space group $P1$ and lattice parameters that are in good agreement with the theoretical values.

Keywords: Calorimetric measurements; Cyclomaltooligosaccharides; Cyclodextrins; Dielectric spectroscopy; Pentaiodide ions; Raman spectroscopy

1. Introduction

The addition of metal iodides (MI_n) and molecular iodine (I_2) to aqueous solutions of cyclomaltohexaose (α-cyclodextrin, α-CD) can form polyiodide inclusion complexes that are crystallized in four different crystalline forms (triclinic, tetragonal, pseudohexagonal, and hexagonal) depending on the counterion's nature and its coordination scheme.[1,2] By means of X-ray analysis, Noltemeyer and Saenger[1,3] have determined in detail the crystal structure of the α-CD polyiodide complexes with cadmium and lithium metals at room temperature. They found that the α-CD molecules are stacked like coins in a roll (head to head), producing dimers in whose tubular cavities nearly linear pentaiodide ions (I_5^-) are embedded. Four of the five iodine atoms are well ordered (full occupancy) forming two I_2 units that are located within the α-CD cavities. The remaining central iodine anion, which is located between the large sides (O(2),O(3) rims) of the opposing α-CD molecules, is disordered in various occupancy ratios. In the polyiodide complex with Cd^{2+}, which is crystallized in the tetragonal crystal form with space group $P4_22_12$, the occupancy ratio of the central I^- ion was 50/50 (Fig. 1a). Thus, the researchers

* Corresponding author. Tel.: +30 210 7274561; fax: +30 210 7274752; e-mail: jpapaioannou@chem.uoa.gr

0008-6215/$ - see front matter © 2007 Elsevier Ltd. All rights reserved.
doi:10.1016/j.carres.2007.05.025

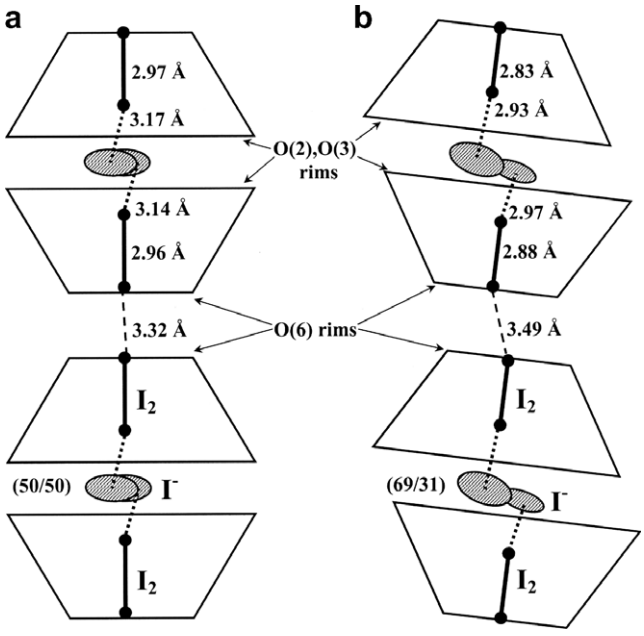

Figure 1. The geometry of the pentaiodide units embedded in the α-CD dimers of (a) the tetragonal $(\alpha\text{-CD})_2{\cdot}Cd_{0.5}{\cdot}I_5{\cdot}27H_2O$ and (b) the triclinic $(\alpha\text{- CD})_2{\cdot}LiI_3{\cdot}I_2{\cdot}8H_2O$, according to the single-crystal X-ray analysis.[1,3] The well-ordered iodine atoms are presented as black spheres. The disordered iodine ions are presented as probability ellipsoids.

rendered the pentaiodide type as $(I_2{\cdot}I^-{\cdot}I_2)$ and the chemical formula as $(\alpha\text{-CD})_2{\cdot}Cd_{0.5}{\cdot}I_5{\cdot}27H_2O$ (named α-Cd in our work). In the case of the polyiodide complex with Li^+ (triclinic $P1$), the occupancy ratio of the disordered I^- ion was 69/31 (Fig. 1b). Therefore, they suggested that each α-CD dimer accommodates two units $I_3^-{\cdot}I_2$ or $I_2{\cdot}I_3^-$ $(I_3^-{\cdot}I_2 \leftrightarrow I_2{\cdot}I_3^-)$ in a statistical ratio of 69:31, and they rendered the chemical formula as $(\alpha\text{-CD})_2{\cdot}LiI_3{\cdot}I_2{\cdot}8H_2O$ (named α-Li in our work). Teitelbaum et al.[4] have carried out a Raman spectroscopy study of the polycrystalline α-Li at room temperature. They observed two bands at 110 and 173 cm^{-1} that were ascribed to the presence of I_3^- ions and weakly coordinated I_2 molecules, respectively. In addition, Mizuno et al.[5] have examined the Raman spectra of the single crystals of α-Cd and α-Li complexes at room temperature. Both samples showed two bands at 107 and 161 cm^{-1} that were attributed to the varied composition of disordered $(I_3^-)_x$ and $(I_5^-)_x$ chains, respectively.

We have recently investigated the Raman spectra of the polycrystalline α-Cd in the temperature ranges of (i) 153–293 K and (ii) 303–383 K,[6] in order to explore the polyiodide variations. It was found that at room temperature, two kinds of pentaiodide units coexist in the polyiodide chain as it was indicated by a strong Raman band at 160 cm^{-1} $(I_2{\cdot}I^-{\cdot}I_2)$ and a shoulder at 168 cm^{-1} $(I_3^-{\cdot}I_2 \leftrightarrow I_2{\cdot}I_3^-)$. The latter signal (168 cm^{-1}) slightly differs from that reported for α-Li (173 cm^{-1}) by Teitelbaum et al.,[4] probably due to the different bond lengths of I_2 units. During the cooling process the shoulder at 168 cm^{-1} disappears, whereas the band at 160 cm^{-1} remains, due to the gradual transformation $(I_3^-{\cdot}I_2 \leftrightarrow I_2{\cdot}I_3^-) \rightarrow (I_2{\cdot}I^-{\cdot}I_2)$. During heating the band at 160 cm^{-1} disappears, and the initial shoulder at 168 cm^{-1} becomes the main band because of the inverse transformation $(I_2{\cdot}I^-{\cdot}I_2) \rightarrow (I_3^-{\cdot}I_2 \leftrightarrow I_2{\cdot}I_3^-)$. These effects are caused by the continuous changes of the occupancy ratio of the disordered I^- ions with temperature. We did not detect the characteristic Raman band ν_1 of I_3^- ions at approximately 105–110 cm^{-1} due to the limited frequency range of the spectrometer ($\geqslant$100 cm^{-1}). Instead of this, we observed the progressive overtones at 211 (2×107) and 312 cm^{-1} (3×107), whose intensity variation followed the intensity variation of the band at 168 cm^{-1} during cooling and heating. This effect verified that the non-detectable band at ~107 cm^{-1} and the band at 168 cm^{-1} originate from the same chemical species $(I_3^-{\cdot}I_2 \leftrightarrow I_2{\cdot}I_3^-)$. The shoulder at 168 cm^{-1} was not reported by Mizuno and co-workers, probably because their research was restricted to only room temperature.

Additionally, we have used dielectric spectroscopy measurements, which provided sufficient information about the electrical conduction of various α-CD polyiodide complexes with different metal ions.[6–8] Specifically, in the temperature range of 120–300 K—where all the water molecules of the crystal lattice exist—the dielectric constant $(\varepsilon', \varepsilon'')$ and the phase shift (φ) of α-Cd and α-Li complexes[7] revealed the following: (i) the well-known order–disorder transition of some normal hydrogen bonds to those of flip-flop type[9,10] and (ii) the existence of two kinds of water molecules (tightly bound, easily movable) in α-Cd and one kind (tightly bound) in α-Li. Furthermore, we have investigated the ac-conductivity and the phase shift of α-Cd over the extended temperature range of 240–425 K[6] in order to detect all the different mechanisms of charge transport that take place in the sample (proton conduction, metallic movements, polyiodide interactions, and dehydration process). It was found that the Arrhenius exponential behaviour of the ac-conductivity in the temperature range of 276.2–377.0 K is not affected by the dehydration process because of the continuous transformation $(H_2O)_{\text{tightly bound}} \rightarrow (H_2O)_{\text{easily movable}}$ and the contribution of the cadmium ions via the water-net. When most of the water molecules have been removed from the lattice, the ac-conductivity decreases rapidly since the already depleted metal ions act as localized charges no longer making a contribution. Finally, an abrupt increase of the ac-conductivity was observed at $T > 413.2$ K due to the sublimation of iodine.

All of the above phenomena are of great scientific interest due to the fact that the hydrogen-bonded networks are systematically studied in biological systems,[11–15] and the polyiodides display potential

technical applications in various areas.[16–18] Since each one of the α-CD polyiodide complexes is expected to present characteristic dielectric properties as a result of the differences in the counterion's nature, the degree of hydration and the pentaiodide formations, in the present work we extend our research to the α-cyclodextrin–pentaiodide inclusion complex with sodium metal (α-Na). The dielectric measurements are carried out over a frequency range of 0–100 kHz and the temperature range of 125–450 K. Besides this, the Raman spectra are investigated in the temperature ranges of (i) 153–298 K and (ii) 303–413 K, and calorimetric measurements are carried out in the range of 273–443 K.

2. Results

2.1. Thermogravimetric analysis (TGA)

The thermogravimetric analysis of α-Na (Fig. 2) with a heating rate of 5 °C/min reveals eight (8) water molecules per α-cyclodextrin dimer, so the general composition is $(\alpha\text{-CD})_2{\cdot}NaI_5{\cdot}8H_2O$. The number of the water molecules was calculated from the weight loss in the temperature range of 70–125 °C where the dehydration process takes place. Figure 3 shows the number of the remaining water molecules per dimer, as the temperature increases.

2.2. X-ray powder diffraction (XRD) and Rietveld analysis

A few grams of polycrystalline α-Na were finely hand-pulverized in order to reduce the greater volume fraction of certain crystal orientations (texture) in the sample. We collected the experimental XRD pattern at room temperature covering the 5–55° 2θ range, in order to perform a Rietveld refinement of the lattice parameters.

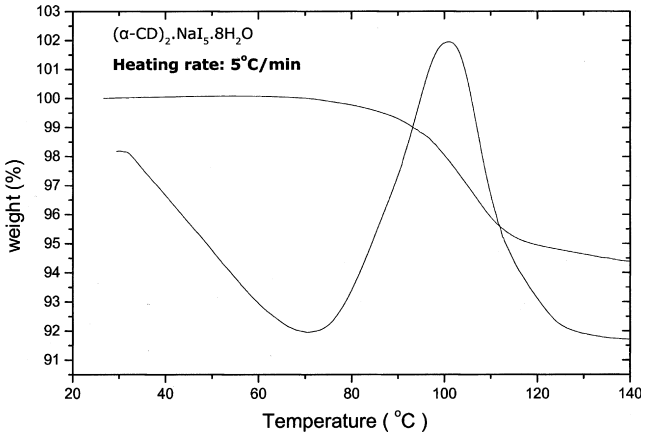

Figure 2. Simultaneous thermogravimetry (TGA) and differential thermal analysis (DTA) of $(\alpha\text{-CD})_2{\cdot}NaI_5{\cdot}8H_2O$, with a heating rate of 5 °C/min.

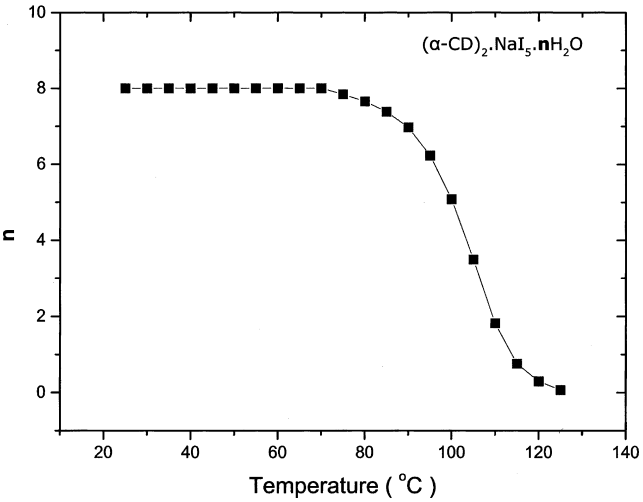

Figure 3. The variation of the number of the remaining water molecules per α-CD dimer in $(\alpha\text{-CD})_2{\cdot}NaI_5{\cdot}8H_2O$ during the heating process.

Figure 4 shows the experimental X-ray powder diffraction pattern. The Rietveld refinement of this profile (POWDER CELL 2.4 software) with the triclinic $P1$ structure of $(\alpha\text{-CD})_2{\cdot}LiI_3{\cdot}I_2{\cdot}8H_2O$[1] is also shown in Figure 4: $R_p = 7.17\%$, $R_{wp} = 10.93\%$, $R_{exp} = 7.97\%$, and $\chi^2 = 1.880$. We obtained a triclinic $P1$ crystal form with the following lattice parameters $a = 13.4800(0)$ Å, $b = 13.9001(7)$ Å, $c = 15.6284(1)$ Å, $\alpha = 93.8542(3)°$, $\beta = 87.8343(0)°$, and $\gamma = 120.351(0)°$, which differ by less than 1% from those values reported by Noltemeyer and Saenger.[1] We note that some experimental peak intensities at room temperature vary from those calculated, mainly due to the fact that the greatest percentage of the pentaiodide ions does not follow the

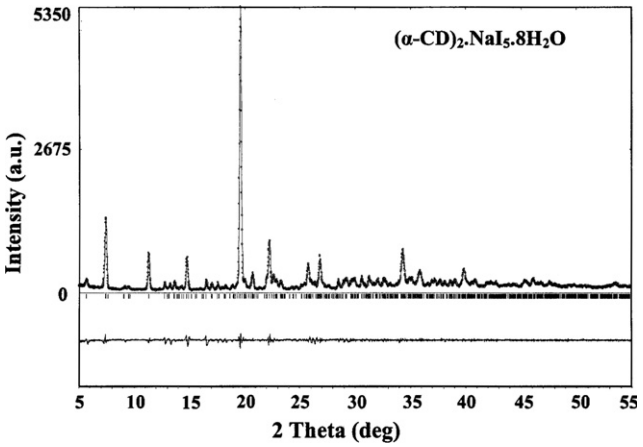

Figure 4. Rietveld refinement pattern of $(\alpha\text{-CD})_2{\cdot}NaI_5{\cdot}8H_2O$. Black circles: experimental pattern, solid line: refined model. The curve at the bottom is the difference between the observed and calculated intensities in the same scale. Black vertical lines indicate the positions of the allowed reflections.

$I_3^-\cdot I_2 \leftrightarrow I_2\cdot I_3^-$ geometry, which was found from the single-crystal X-ray analysis of α-Li.[1] This structural change becomes obvious from the Raman spectroscopy study. The observed isomorphism between the α-Na and α-Li complexes indicates that the coordination scheme of the Na^+ ions is similar to that of the Li^+ ions (four OH-groups and a H_2O molecule in a square pyramidal form). Noltemeyer and Saenger[1] have shown that the cations Li^+, Na^+, and Tl^+ have the ability to interact with the α-CD hydroxyl groups, forming isomorphous crystal structures (triclinic *P*1). Finally, the total absence of any hump (indicative of amorphous material) in the experimental pattern proves the purity of the synthesized sample (single phase).

2.3. Dielectric spectroscopy

The temperature dependence of the dielectric constant $(\varepsilon', \varepsilon'')$ of α-Na over the range of 125–342 K, at a frequency of 300 Hz, is shown in Figure 5. The real part ε' increases in an extended and well-distinguished single sigmoid fashion from 6.4 at 125.3 K to 31.3 at 278.3 K with an inflection point observed at 207.6 K ($\varepsilon' = 17.3$). Above 278.3 K, ε' increases rapidly to the value $\varepsilon' = 57.7$ at 341.6 K. The imaginary part ε'' presents a slab bell-shaped curve with peak value $\varepsilon'' = 3.6$ at 211.2 K, whereas at $T > 278.3$ K it increases rapidly to the value of 33.8 at 341.6 K.

Figure 6 shows the phase shift φ of α-Na at a fixed frequency of 300 Hz, over the temperature range of 125–450 K. Specifically, it drops from 86.7° at 125.3 K to a minimum value of 77.3° at 200.9 K, then it increases to 84.3° at 266.5 K, whereas at $T > 281.4$ K it decreases abruptly to a second minimum value of 30.9° at 388.9 K; then it increases again to 53.8° at 414.9 K and finally drops to 4.8° at 447.9 K. At higher fixed frequencies (1–100 kHz), the $\varepsilon'(T)$, $\varepsilon''(T)$ and $\varphi(T)$ variations present similar behaviour.

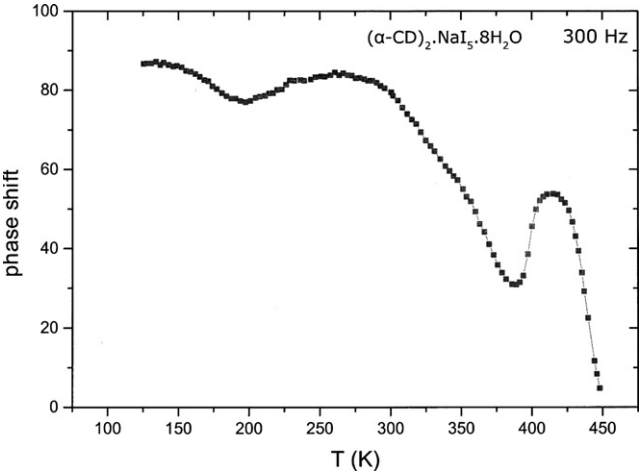

Figure 6. Temperature dependence of the phase shift (φ) of $(\alpha\text{-CD})_2\cdot NaI_5\cdot 8H_2O$ at 300 Hz.

The temperature variation of the ac-conductivity ($\ln\sigma$ vs $1/T$) of α-Na during the heating process under an applied frequency of 300 Hz is shown in Figure 7. This plot presents the sigmoid curve (a) in the temperature range $3.59\ K^{-1} < 10^3/T < 7.98\ K^{-1}$ and the linear parts (b), (c) in the temperature ranges $2.80\ K^{-1} < 10^3/T < 3.59\ K^{-1}$ and $2.59\ K^{-1} < 10^3/T < 2.80\ K^{-1}$, respectively. At $10^3/T < 2.59\ K^{-1}$ there is an abrupt decrease to a topical minimum value at $10^3/T = 2.41\ K^{-1}$ and then a rapid increase up to $10^3/T = 2.23\ K^{-1}$.

The impedance plot ImZ versus ReZ (0–100 kHz) of α-Na in the temperature range of 287.2–391.5 K (Fig. 8a and b) shows circular arcs whose radii continuously decrease up to 385.9 K and then increase at

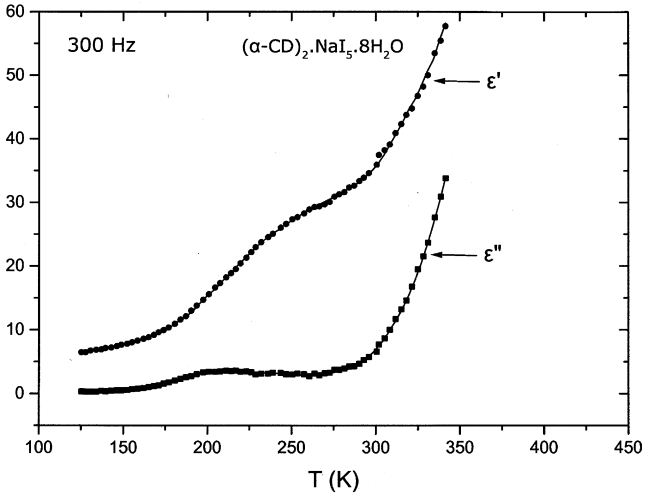

Figure 5. Temperature dependence of the real (ε') and imaginary (ε'') part of the dielectric constant of $(\alpha\text{-CD})_2\cdot NaI_5\cdot 8H_2O$ at 300 Hz.

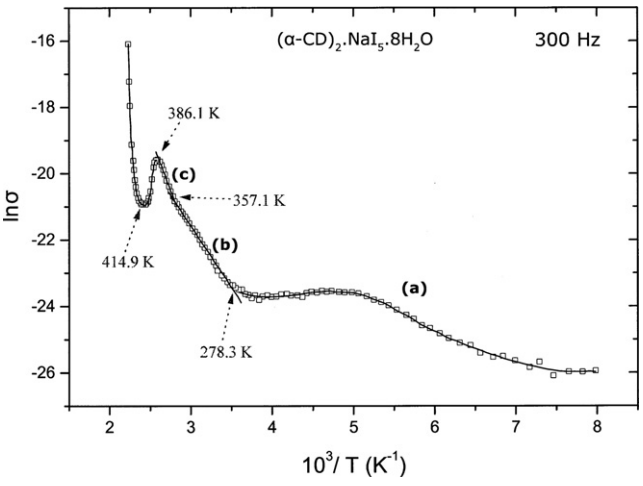

Figure 7. Temperature dependence of the ac-conductivity ($\ln\sigma$ vs $1/T$) of $(\alpha\text{-CD})_2\cdot NaI_5\cdot 8H_2O$ at 300 Hz.

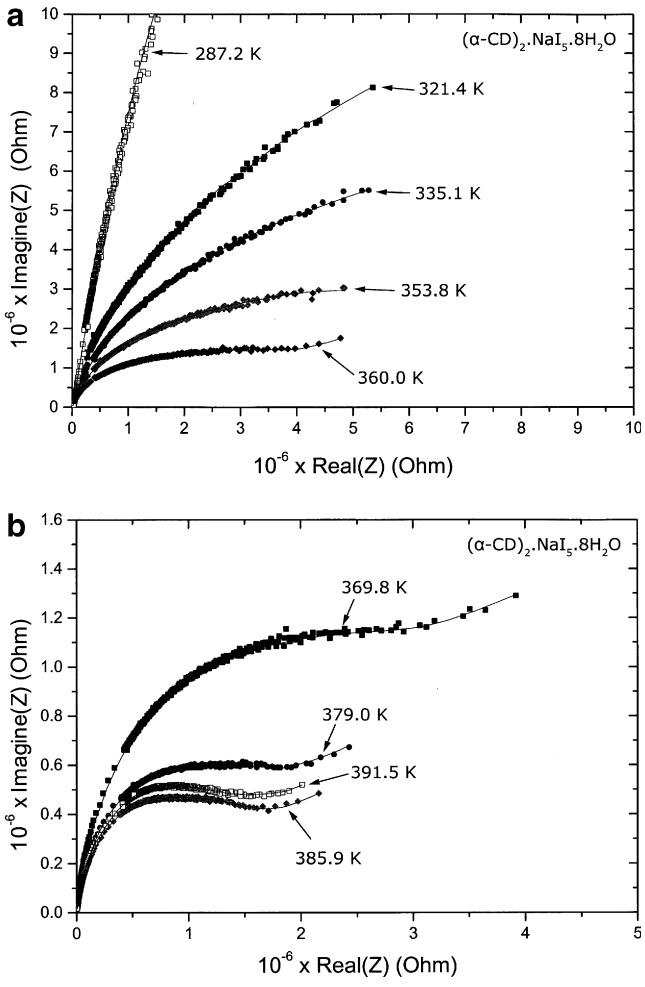

Figure 8. Impedance plot of $(\alpha\text{-CD})_2{\cdot}NaI_5{\cdot}8H_2O$ in the temperature ranges of (a) 287.2–360.0 K and (b) 369.8–391.5 K.

391.5 K. The linear segment which is generated in the low-frequency region at $T \sim 360$ K becomes well distinguished at higher temperatures.

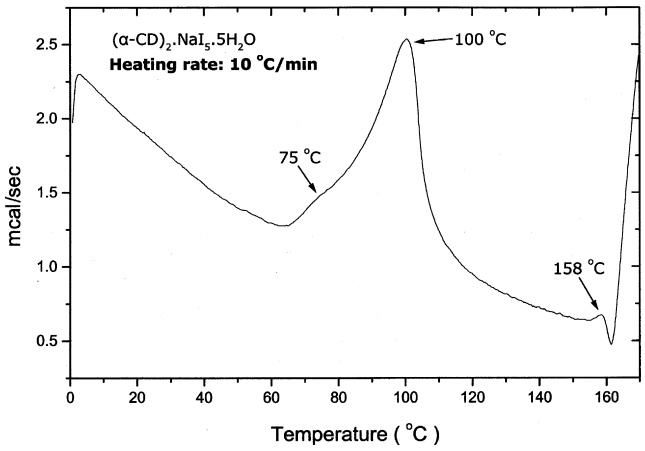

Figure 9. DSC thermogram of $(\alpha\text{-CD})_2{\cdot}NaI_5{\cdot}8H_2O$ with a heating rate of 10 °C/min.

2.4. Differential scanning calorimetry (DSC)

The DSC trace of α-Na in Figure 9, recorded with a scan rate of 10 °C min^{-1}, shows a small shoulder and a strong endothermic peak with onset temperatures 75 and 100 °C, respectively. At 158 °C a small peak is observed, followed by an upward baseline which indicates the decomposition of the sample.

2.5. Raman spectroscopy

The Raman spectra of α-Na during the cooling process in the range of −120 to 25 °C are shown in Figure 10a and b. Initially, at 25 °C there is only one strong band at 160 cm^{-1} with an intensity of 41.04. As the

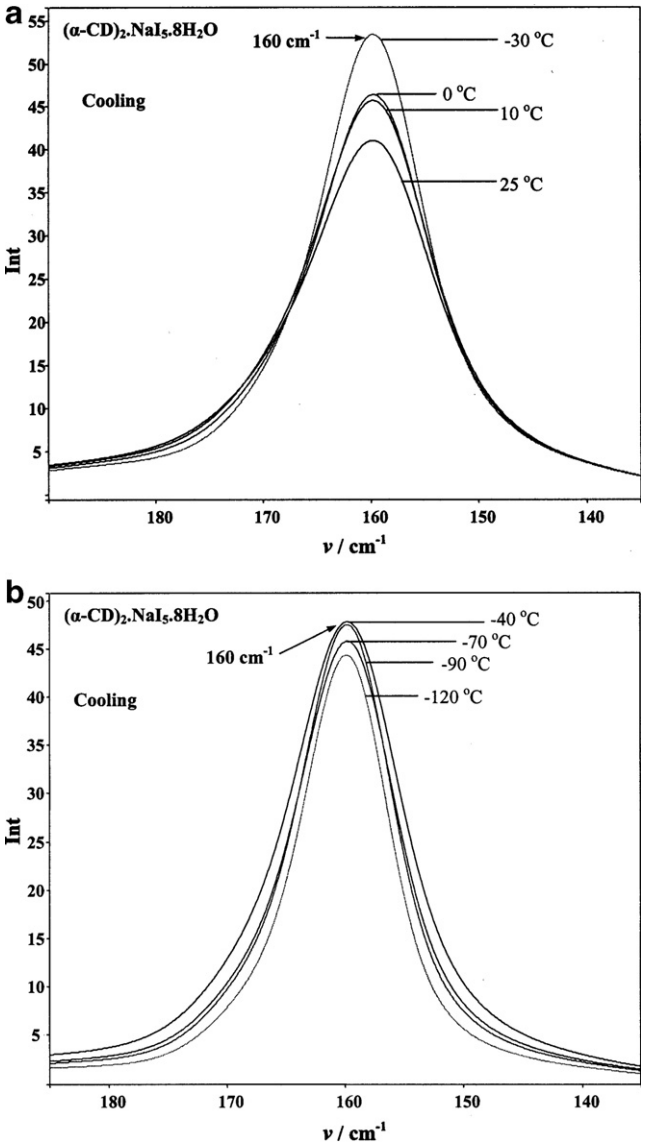

Figure 10. Raman spectra of $(\alpha\text{-CD})_2{\cdot}NaI_5{\cdot}8H_2O$ during cooling, in the temperature ranges of (a) −30 to 25 °C and (b) −120 to −40 °C.

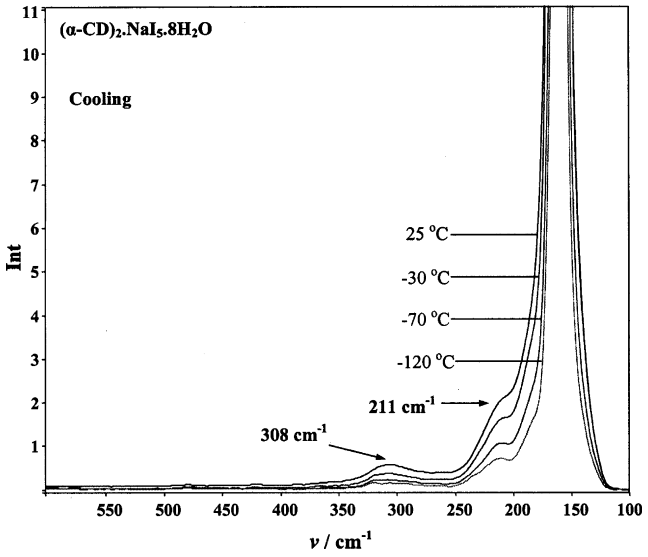

Figure 11. Raman overtones of $(\alpha\text{-CD})_2{\cdot}NaI_5{\cdot}8H_2O$ during cooling, at the representative temperatures of 25, −30, −70, and −120 °C.

temperature decreases the intensity increases to the value of 53.37 at −30 °C. From −40 up to −120 °C, the intensity of the band at 160 cm^{-1} fluctuates between the values of 44 and 48. Figure 11 shows the Raman spectra during cooling at the representative temperatures of 25, −30, −70 and −120 °C, in the extended frequency range of 100–600 cm^{-1}. Two more bands are observed at 211 cm^{-1} and 308 cm^{-1} whose intensities gradually decrease, as the temperature is lowered up to −120 °C.

The Raman spectra of α-Na during the heating process in the range of 30–140 °C are shown in Figure 12a–d. At 30 °C there is a strong band at 160 cm^{-1} with an intensity of 39.33 and a shoulder at 169 cm^{-1} with an intensity of 26.79. At 40 °C the intensities of the strong band and the shoulder decrease to the values of 26.08 and 18.12, respectively. At 50 °C the intensity of the band at 160 cm^{-1} decreases to 20.45, whereas the intensity of the shoulder at 169 cm^{-1} increases to 21.68. At 60 °C the initial shoulder becomes a strong band at 169 cm^{-1} with an intensity of 17.07, whereas the initial band at 160 cm^{-1} becomes a shoulder with an intensity of 12.57. From 70 up to 120 °C, the intensities of these two bands continuously decrease. At 130–140 °C, there is a strong band at 172 cm^{-1}, whereas the shoulder at 160 cm^{-1} still remains. Figure 13 shows the Raman spectra during heating at the representative temperatures of 30, 40, 50, and 70 °C in the extended frequency range of 100–650 cm^{-1}. From 30 up to 40 °C, the intensities of the bands at 211 cm^{-1} and 308 cm^{-1} decrease from 3.78 to 2.86 and from 1.08 to 0.88, respectively. At 50 °C they increase taking the values of 4.18 and 2.53, whereas at 70 °C they decrease again to 2.80 and 2.03, respectively.

3. Discussion

3.1. Charge transport properties

All the different electrical conduction mechanisms that take place in the temperature range of 125–450 K are clearly depicted in the $\ln\sigma$ versus $1/T$ plot (Fig. 7). Specifically, the extended sigmoid (a) in the temperature range of 125.3–278.3 K is caused by the well-known order–disorder transformation[9,10] of some normal hydrogen bonds to those of flip-flop type during the heating process. Generally, the flip-flop hydrogen bonds of the cyclodextrin complexes produce extended chains that consist of disordered water molecules and hydroxyl groups. In the present case, the fact that a second sigmoid was not observed indicates the existence of only one kind of water molecule (tightly bound) in the above temperature region, as in the case of the isomorphous α-Li.[7] This conclusion is also confirmed by the existence of a single step, a single bell-shaped peak and a single minimum value at $T < 278.3$ K in the $\varepsilon'(T)$, $\varepsilon''(T)$, and $\varphi(T)$ variations, respectively. The order–disorder transition temperature is 200.9 K as it is found by the topical minimum of the phase shift (Fig. 6).

The linear part (b) in the range of 278.3–357.1 K shows an Arrhenius behaviour according to $\sigma = \sigma_0 \exp(-E_a/k_B T)$, with activation energy $E_a = 0.32$ eV. This exponential increment of the ac-conductivity is a result of the continuous transformation:

$$(H_2O)_{\text{tightly bound}} \rightarrow (H_2O)_{\text{easily movable}} \quad (1)$$

which gradually increases the number of the mobile charge carriers (reorientated H_2O dipoles) in the crystal lattice. This procedure is also responsible for the abrupt increase of ε', ε'' and the rapid decrease of φ at approximately $T > 278.3$ K. Figure 3 shows that in the temperature range of 343–353 K (70–80 °C), very few easily movable water molecules have been removed from the sample as it is also confirmed by the small endothermic shoulder of the DSC trace at 348 K (75 °C) over the same range (Fig. 9). At ~353 K, the remaining tightly bound water molecules start to escape from the lattice as evident from the strong DSC peak with onset temperature 373 K (100 °C). It has been shown[19–21] that the progressive dehydration process reduces the concentration of the mobile water molecules in the sample, resulting in a lower increasing rate (lower E_a) of the conductivity. However, the ac-conductivity of α-Na follows the Arrhenius behaviour without any deviation until 357.1 K (84.1 °C) because of the gradual transformation 1 which counterbalances the reduction of the easily movable water molecules.

The linear part (c) in the range of 357.1–386.1 K also follows the Arrhenius law, presenting an activation energy of 0.55 eV, which is greater than that of the linear part (b). That happens because the contribution of the

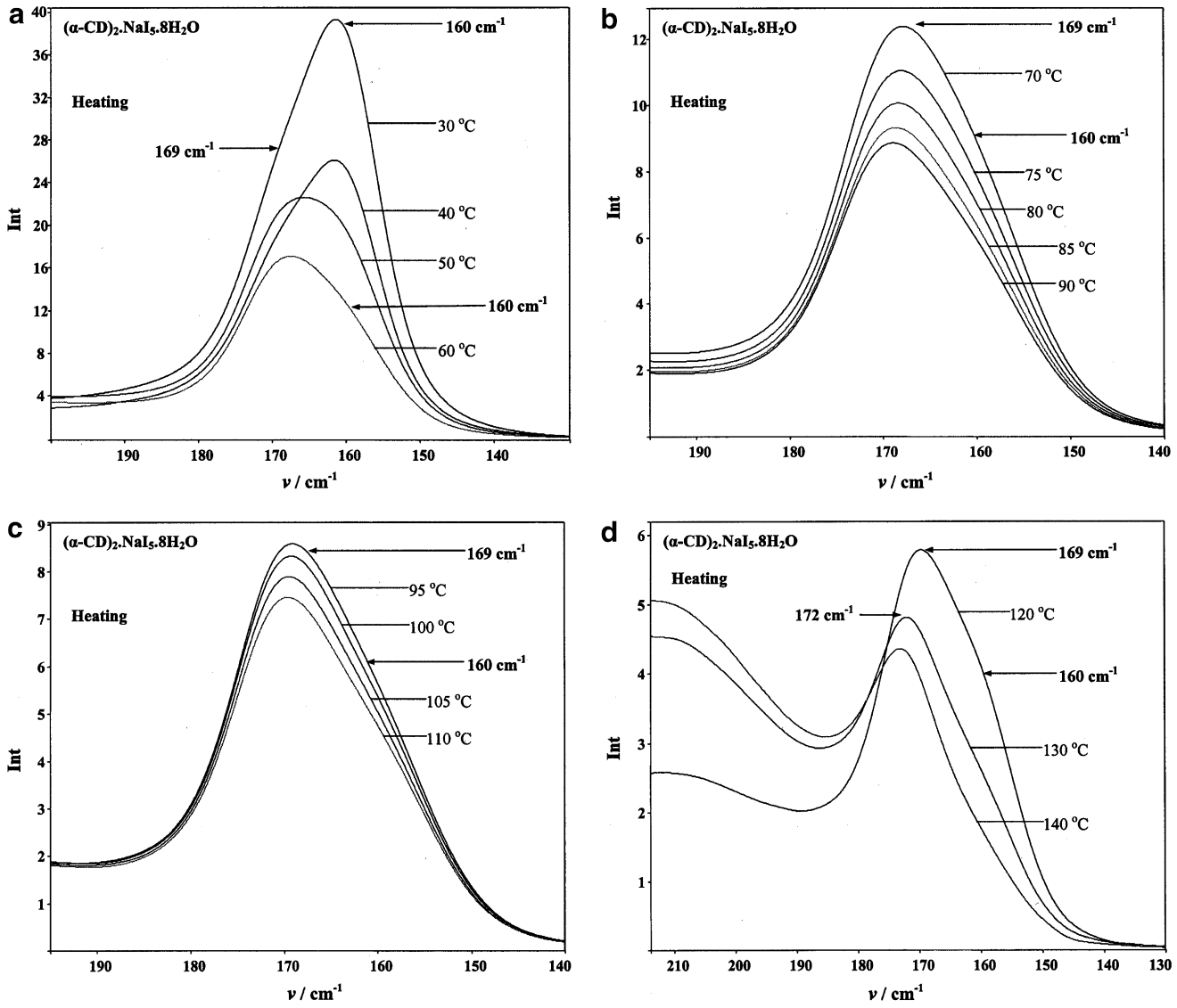

Figure 12. Raman spectra of $(\alpha\text{-CD})_2{\cdot}NaI_5{\cdot}8H_2O$ during heating, in the temperature ranges of (a) 30–60 °C, (b) 70–90 °C, (c) 95–110 °C, and (d) 120–140 °C.

water network is amplified by the sodium ions' movements, as it is indicated by the impedance plot. At $T<$ 360 K, where the Na^+ ions are restricted by four hydroxyl groups and one water molecule in a square pyramidal form,[1] the continuously decreased radii of the circular arcs in Figure 8a are exclusively attributed to the continuous transformation 1. This thermally activated process results in a gradual reduction of the grain interior impedance. The generated linear segment in the low-frequency region at ~360 K reveals the onset of space charge in the material.[21–23] This phenomenon is directly related to the released Na^+ ions, which oscillate with the frequency of the applied field, contributing to the ac-conductivity. This contribution is facilitated via a chemical exchange of H^+ in the water-net, described as the deGrotthuss mechanism.[15,24–26]

The rapid decrease of the ac-conductivity at $T>$ 386.1 K is due to the fact that most of the water molecules have been removed from the crystal lattice (~1.8 remaining molecules per dimer according to Fig. 3) causing a significant attenuation of the proton conduction. Additionally, the breakdown of the water-net minimizes the contribution of the sodium ions that act as localized charges. For these reasons, the phase shift rises in the temperature range of 388.9–414.9 K (Fig. 6), and the radii of the circular arcs increase at 391.5 K in the impedance plot (Fig. 8b).

Finally, the abrupt increase of σ at $T>414.9$ K is caused by the sublimation of iodine, which is also evident from the small endothermic peak with onset temperature 431 K (158 °C) in the DSC trace (Fig. 9). This process provides conductive paths[27] along the

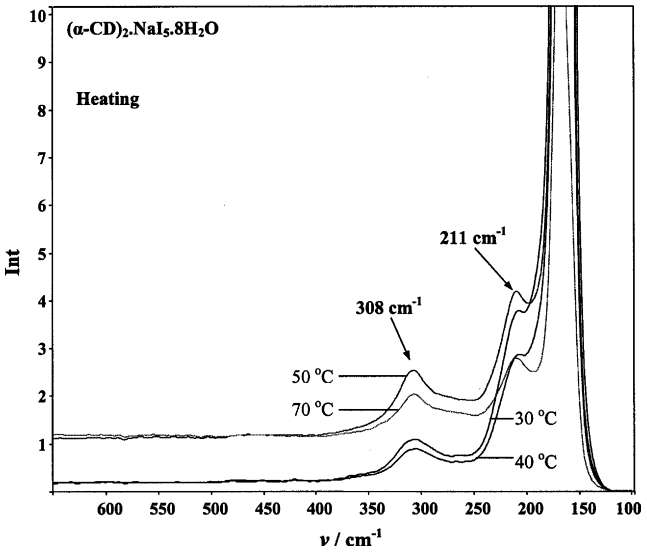

Figure 13. Raman overtones of $(\alpha\text{-CD})_2{\cdot}NaI_5{\cdot}8H_2O$ during heating, at the representative temperatures of 30, 40, 50, and 70 °C.

polyiodide chains, resulting in an increase in connectivity and strong electron interactions between the neighboring I_5^- units. As the temperature increases, the effusion of the sublimed iodine molecules causes the rupture of the grain boundaries. This effect is responsible for the upward baseline above 435 K (162 °C) in the DSC trace. We clarify that this procedure should not be related to the decomposition of the α-cyclodextrin molecules. According to Bettinetti et al.,[28] the decomposition of α-CDs begins at temperatures higher than 523 K.

3.2. Pentaiodide transformations

From the dielectric measurements, it becomes apparent that the polyiodide chains make an essential contribution to the ac-conductivity at $T > 414.9$ K. All the pentaiodide variations up to the sublimation of iodine are depicted in the Raman spectroscopic results. As in the case of α-Cd,[6] two kinds of pentaiodide units ($I_2{\cdot}I^-{\cdot}I_2$ and $I_3^-{\cdot}I_2 \leftrightarrow I_2{\cdot}I_3^-$) are detected during the thermal examination of the sample. At room temperature (25 °C), there is only one strong band at 160 cm^{-1}, indicating that the polyiodide chains exclusively consist of ($I_2{\cdot}I^-{\cdot}I_2$) units.[4,5,18,29–31] However, the observed overtones of the I_3^- ions at 211 cm^{-1} (2×107) and 308 cm^{-1} (3×107) (Fig. 11) reveal that besides the ($I_2{\cdot}I^-{\cdot}I_2$) units there are also some pentaiodides of ($I_3^-{\cdot}I_2 \leftrightarrow I_2{\cdot}I_3^-$) type. The expected band at ~170 cm^{-1}, which corresponds to the ν_1 of the weakly coordinated I_2 of this type,[6,18,32] is obscured by the strong band at 160 cm^{-1}, indicating a negligible ($I_3^-{\cdot}I_2 \leftrightarrow I_2{\cdot}I_3^-$) population at room temperature (at higher temperatures this weak band becomes intense and well distinguished, presenting a frequency of 169 cm^{-1}).

The gradually decreased intensity of the I_3^- overtones in the Raman spectra during the cooling process (Fig. 11) indicates the progressive transformation:

$$(I_3^-{\cdot}I_2 \leftrightarrow I_2{\cdot}I_3^-) \rightarrow (I_2{\cdot}I^-{\cdot}I_2) \quad (2)$$

This transformation is due to the fact that the occupancy ratio of the disordered I^- ions in the ($I_3^-{\cdot}I_2 \leftrightarrow I_2{\cdot}I_3^-$) units continuously changes from an initial value of, for example, …60/40…70/30… to the final value of 50/50 as the temperature decreases. All of these effects are explicitly shown in Figure 14, where the ($I_3^-{\cdot}I_2 \leftrightarrow I_2{\cdot}I_3^-$) units are presented as form (I). The ($I_2{\cdot}I^-{\cdot}I_2$) units are displayed by the 2 equiv forms (IIa) and (IIb), which remain unaffected during cooling. In form (IIa) the central I^- ion is twofold disordered in occupancy ratio 50/50, whereas in form (IIb) the central I^- ion is well ordered (full occupancy) and equidistant from the two I_2 molecules. This distinction is clarified by the following discussion of the Raman spectra during heating.

At 30 °C the band at 169 cm^{-1} is well distinguished (strong shoulder), coexisting with the main band at 160 cm^{-1} (Fig. 12a). As the temperature increases the band at 169 cm^{-1} becomes more intense in comparison to that at 160 cm^{-1}. Thus, at 60 °C we observe a main band at 169 cm^{-1} and a shoulder at 160 cm^{-1}. This relative intensity change is caused by the transformation

$$(I_2{\cdot}I^-{\cdot}I_2) \rightarrow (I_3^-{\cdot}I_2 \leftrightarrow I_2{\cdot}I_3^-) \quad (3)$$

which implies a progressive change of the occupancy ratio of the I^- ions in the initial (25 °C) form (IIa), from 50/50 to the value of …60/40…70/30… and so on (Fig. 14). Similar changes also happen to the occupancy ratio of the I^- ions in the initial (25 °C) form (I) (e.g., …60/40…70/30…→…70/30…80/20…). Therefore, it appears to be explicit that as the temperature increases the vario-occupancy ratio of the disordered ions I^- in the pentaiodide forms (I) and (IIa) presents the tendency to take the value of 100/0 (this ratio does not really exist. It is merely a creation on the part of the authors in order to illustrate full occupancy). It is obvious that the disordered I^- ions in form (I) will become well ordered earlier than those in form (IIa), according to the order–disorder transition

$$\underset{\text{(disordered } I^-)}{(I_3^-{\cdot}I_2 \leftrightarrow I_2{\cdot}I_3^-)} \rightarrow \underset{\text{(well-ordered } I^-)}{(I_3^-{\cdot}I_2)} \quad (4)$$

This transition indicates a charge transfer interaction between the I^- ion (Lewis base donor) and one of the two I_2 molecules (Lewis acid acceptors). This effect can be detected by the $\varphi(T)$ variation as was shown in the case of α-Cd,[6] where a topical minimum of φ was observed at 404.3 K (before the sublimation of iodine). In the present case, we did not observe any topical min-

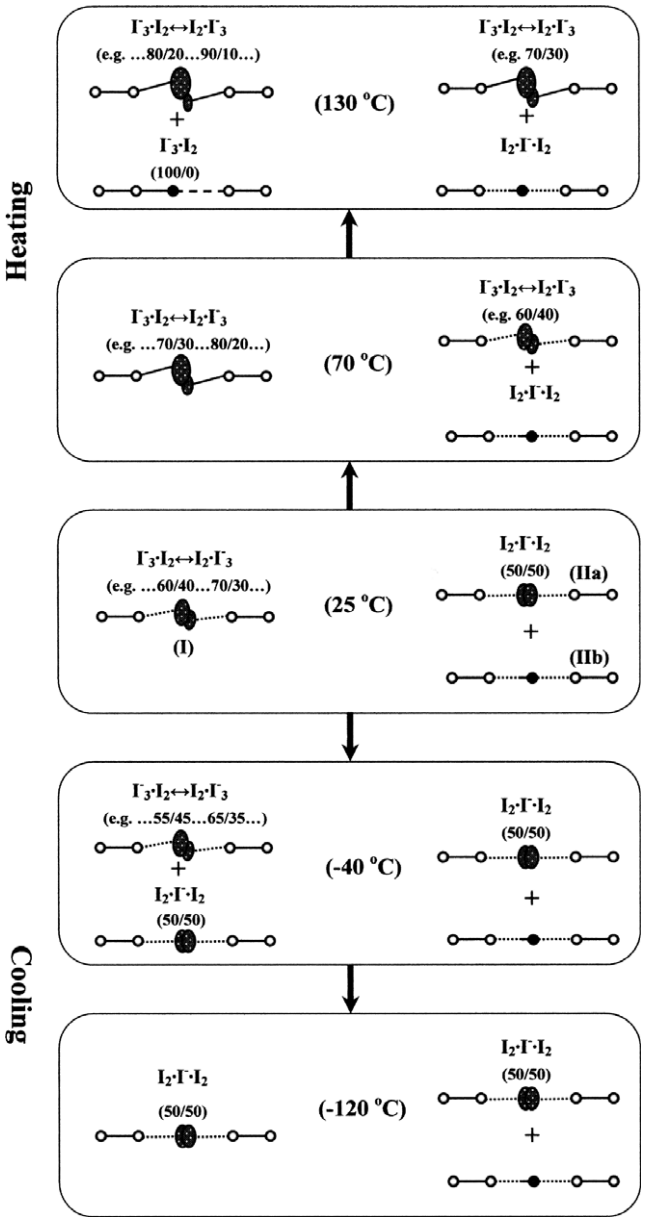

Figure 14. The coexistence of the two pentaiodide forms $I_2{\cdot}I^-{\cdot}I_2$ and $I_3^-{\cdot}I_2 \leftrightarrow I_2{\cdot}I_3^-$ in $(\alpha\text{-CD})_2{\cdot}NaI_5{\cdot}8H_2O$ at 25 °C and the progressive variation of the occupancy ratio (x/y) of the disordered I^- ions as the temperature decreases up to −120 °C and as the temperature increases up to 130 °C. The disordered I^- ions are presented as dashed ellipsoids. The size of each ellipsoid is determined by the corresponding amount of each ratio. The well-ordered I^- ions are presented as black spheres. The ratio 100/0 indicates full occupancy (well-ordered I^- ions).

imum of φ at approximately 405 K. That happens because the population of form (I) is negligible at 25 °C, and at elevated temperatures the transition 4 is limited in the polyiodide chains. On the contrary, in α-Cd there was a great population (I) at room temperature, which resulted in a strong charge-transfer interaction at 404.3 K.

The population of form (IIb) remains unaffected during heating, retaining the shoulder at 160 cm^{-1} in the

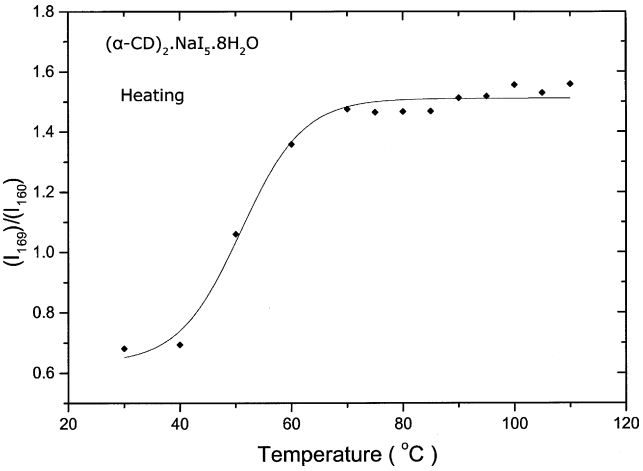

Figure 15. The temperature dependence of the Raman intensity ratio I_{169}/I_{160} of $(\alpha\text{-CD})_2{\cdot}NaI_5{\cdot}8H_2O$ during the heating process.

range of 70–130 °C. Figure 15 shows the variation of the intensity ratio I_{169}/I_{160} with temperature. From 30 up to 70 °C, this ratio increases due to the gradual transformation 3. In this temperature region, the intensity variation of the I_3^- overtones (Fig. 13) follows the intensity variation of the band at 169 cm^{-1}. This effect shows that the non-detectable band at ~107 cm^{-1} and the band at 169 cm^{-1} originate from a single chemical species ($I_3^-{\cdot}I_2 \leftrightarrow I_2{\cdot}I_3^-$).[6,31] Above 70 °C, the transformation 3 is completed, resulting in an almost constant I_{169}/I_{160} ratio (Fig. 15).

All of the above Raman spectral data provide sufficient information about the polyiodide structural changes with temperature, indicating that the occupancy ratio of the disordered I^- ions determines the predominant pentaiodide form. The question that could be raised at this point is what kind of disorder do we observe, dynamic, static or a combination of them? The most effective way to discriminate between these two kinds of disorder is the detailed crystallographic study (X-ray or neutron diffraction) over a range of temperatures, by an expert.[9,33–35] Specifically, the neutron diffraction analysis would also determine the interactions between the O(2),O(3) hydrogen atoms H and the disordered I^- ions. Such O–H···I^- interactions have been recently reported for the α-cellobiose2NaI·2H_2O complex[36] and for the cyclomaltohexaicosaose triiodide inclusion complex.[37]

4. Conclusions

Dielectric spectroscopy is an effective method to detect all the different electrical conduction mechanisms that take place in $(\alpha\text{-CD})_2{\cdot}NaI_5{\cdot}8H_2O$ during the heating process. This becomes evident from the $\ln\sigma$ versus $1/T$ plot. Specifically:

(i) The extended sigmoid (a) in the range of 125.3–278.3 K reveals the well-known order–disorder transformation of some normal hydrogen bonds to those of the flip-flop type at 200.9 K and the existence of only one kind of water molecules (tightly bound).
(ii) The linear part (b) in the range of 278.3–357.1 K shows the continuous transformation $(H_2O)_{\text{tightly bound}} \rightarrow (H_2O)_{\text{easily movable}}$ with activation energy $E_a = 0.32$ eV. This transformation counterbalances the reduction of the water molecules during the dehydration process.
(iii) The linear part (c) in the range of 357.1–386.1 K presents a greater activation energy ($E_a = 0.55$ eV) than that of the linear part (b) revealing the sodium ions' contribution to the ac-conductivity. This contribution is facilitated via the water-net.
(iv) At $T > 386.1$ K the ac-conductivity decreases rapidly due to the dehydration process that turns the sodium ions into localized charges and attenuates the proton conduction.
(v) Finally, the abrupt increase of the ac-conductivity at $T > 414.9$ K is caused by the sublimation of iodine, which results in strong electron interactions between the neighboring I_5^- units.

Additionally, the Raman spectroscopy provides complementary information about the polyiodide structural changes with temperature. Two kinds of pentaiodide units ($I_2 \cdot I^- \cdot I_2$) and ($I_3^- \cdot I_2 \leftrightarrow I_2 \cdot I_3^-$) coexist in the polyiodide chain of α-Na at room temperature, as indicated by the characteristic Raman bands at 160 and 169 cm^{-1}, respectively. The ($I_3^- \cdot I_2 \leftrightarrow I_2 \cdot I_3^-$) units are presented as form (I), and their central I^- ion is disordered in occupancy ratio different from 50/50 (e.g., …60/40…70/30…). The ($I_2 \cdot I^- \cdot I_2$) units are displayed by the 2 equiv forms (IIa) and (IIb). In (IIa) the central I^- ion is twofold disordered in occupancy ratio 50/50. In (IIb) the central I^- ion is well ordered and equidistant from the two I_2 molecules. At low temperatures, the transformation (I)→(IIa) takes place, whereas at high temperatures the inverse one (IIa)→(I) happens. All of these effects are caused by the continuous changes of the occupancy ratio of the disordered I^- ions with temperature.

5. Experimental

5.1. Materials and synthesis

α-Cyclodextrin, iodine, and sodium iodide were obtained from Fluka Chemica. α-CD (5.50 g, 5.66 mmol) were dissolved in distilled water (40 mL) at room temperature under stirring until the solution became almost saturated. Then 0.17 g of sodium iodide (1.13 mmol) and 0.22 g of solid iodine (0.866 mmol) were added simultaneously to the solution, and it was heated to 70 °C for 20–25 min. The hot solution was transferred quickly through a folded filter to an empty beaker (100 mL) that was covered with Teflon and then immersed in a Dewar flask (500 mL) containing water at the same temperature. After two days, very fine thin needles of α-Na were grown with a dark brown-black color and uniform composition. These were separated in a Buchner filter and dried in air.

5.2. Characterization methods of the synthesized inclusion complex

5.2.1. Thermogravimetric analysis (TGA). Thermogravimetric analysis of the crystals was performed using a NETZSCH-STA 409 EP Controller TASC 414/3 (reference Al_2O_3). The sample (101.20 mg) was heated in the temperature range of 20–140 °C with a heating rate of 5 °C min^{-1}.

5.2.2. X-ray powder diffraction and Rietveld analysis. The experimental X-ray powder diffraction pattern was obtained with a Siemens D 5000 diffractometer ($Cu_{K\alpha1,K\alpha2}$ radiation, in 0.015° steps with a dwell time of 10 s/step, scan range: 5–55° 2θ, monochromator: graphite crystal). The calculation of the simulated X-ray powder diffraction pattern of $(\alpha\text{-CD})_2 \cdot LiI_3 \cdot I_2 \cdot 8H_2O$ and the Rietveld refinement of the lattice parameters were performed by the computer program POWDER CELL 2.4 developed by Nolze and Kraus.[38,39]

5.3. Techniques

5.3.1. Differential scanning calorimetry (DSC). The differential scanning calorimetry method (Perkin–Elmer DSC-4 instrument) was used with a thermal analysis data station (TADS) system for all calorimetric measurements. Known weights (10–16 mg) of α-Na were sealed into aluminum pans and then heated from 0 up to 170 °C, with a heating rate of 10 °C min^{-1}, in a dynamic nitrogen atmosphere.

5.3.2. Dielectric spectroscopy. For dielectric spectroscopy a pressed pellet of powdered sample, 20 mm in diameter with thickness 1.05 mm, was prepared with a pressure pump (Riken Powder model P-1B) at room temperature. Two platinum foil electrodes were pressed at the same time with the sample. The electrical measurements were taken using a low-frequency (0–100 kHz) dynamical signal analyzer (DSA-Hewlett-Packard 3561A) at a temperature range of 125–450 K. The data was transferred to a personal computer through an HP 82335 Interface Bus (IEEE-488), where it was stored and analysed by a software program

(2PLT-1996). An analytical description of the process is given in previous articles.[19,40]

5.3.3. Raman spectroscopy. The Raman spectra were obtained at $4\,cm^{-1}$ resolution from $3500\,cm^{-1}$ to $100\,cm^{-1}$ with a data point interval of $1\,cm^{-1}$ using a Perkin–Elmer NIR FT spectrometer (Spectrum GX II) equipped with an InGaAs detector. The laser power and spot (Nd: YAG at 1064 nm) were controlled to be constant at 50 mW during the measurements, and 400 scans were accumulated. Two experiments were performed in the temperature ranges of (a) −120 to 25 °C and (b) 30–140 °C, with different samples. During the cooling process, the sample was enclosed in a glassy tube and held at a constant temperature (±1 °C) by means of a low-temperature cell (Ventacon).

Acknowledgements

This work was carried out in partial fulfilment of the requirements for V.G.C.'s Ph.D. Thesis. It was partly supported by Grant No. 70/4/3347SARG, NKUA. Professor K. Viras is kindly acknowledged for his assistance in conducting the Raman spectra and calorimetric measurements.

References

1. Noltemeyer, M.; Saenger, W. *J. Am. Chem. Soc.* **1980**, *102*, 2710–2722.
2. Betzel, C.; Hingerty, B.; Noltemeyer, M.; Weber, G.; Saenger, W.; Hamilton, J. A. *J. Inclusion Phenom. Macrocyclic Chem.* **1983**, *1*, 181–191.
3. Noltemeyer, M.; Saenger, W. *Nature* **1976**, *259*, 629–632.
4. Teitelbaum, R. C.; Ruby, S. L.; Marks, T. J. *J. Am. Chem. Soc.* **1980**, *102*, 3322–3328.
5. Mizuno, M.; Tanaka, J.; Harada, I. *J. Phys. Chem.* **1981**, *85*, 1789–1794.
6. Charalampopoulos, V. G.; Papaioannou, J. C.; Tampouris, K. E. *Solid State Ionics* **2007**, *178*, 793–799.
7. Ghikas, T. C.; Papaioannou, J. C. *Mol. Phys.* **2002**, *100*, 673–679.
8. Papaioannou, J. C.; Ghikas, T. C. *Mol. Phys.* **2003**, *101*, 2601–2608.
9. Betzel, C.; Saenger, W.; Hingerty, B. E.; Brown, G. M. *J. Am. Chem. Soc.* **1984**, *106*, 7545–7557.
10. Zabel, V.; Saenger, W.; Mason, S. A. *J. Am. Chem. Soc.* **1986**, *108*, 3664–3673.
11. Nagle, J. F.; Morowitz, H. J. *Proc. Natl. Acad. Sci. U.S.A.* **1978**, *75*, 298–302.
12. Nagle, J. F. *J. Bioenerg. Biomembr.* **1987**, *19*, 413–426.
13. Roux, B.; Karplus, M. *Annu. Rev. Biophys. Biomol. Struct.* **1994**, *23*, 731–761.
14. Quigley, E. P.; Quigley, P.; Crumrine, D. S.; Cukierman, S. *Biophys. J.* **1999**, *77*, 2479–2491.
15. Pomes, R.; Roux, B. *Biophys. J.* **2002**, *82*, 2304–2316.
16. Salaneck, W. R.; Thomas, H. R.; Bigelow, R. W.; Duke, C. B.; Plummer, E. W.; Heeger, A. J.; Macdiarmind, A. G. *J. Chem. Phys.* **1980**, *72*, 3674–3678.
17. Owens, B. B.; Bottelberghe, J. R. *Solid State Ionics* **1993**, *62*, 243–249.
18. Svensson, P. H.; Kloo, L. *Chem. Rev.* **2003**, *103*, 1649–1684.
19. Charalampopoulos, V. G.; Papaioannou, J. C. *Mol. Phys.* **2005**, *103*, 2621–2631.
20. Charalampopoulos, V. G.; Papaioannou, J. C.; Karayianni, H. S. *Solid State Sci.* **2006**, *8*, 97–103.
21. Papaioannou, J. C.; Charalampopoulos, V. G.; Xynogalas, P.; Viras, K. *J. Phys. Chem. Solids* **2006**, *67*, 1379–1386.
22. Jonscher, A. K. *J. Mater. Sci.* **1978**, *13*, 553–562.
23. Macdonald, J. R. *Impedance Spectroscopy*; Wiley: New York, 1987, p 252.
24. de Grotthuss, C. J. T. *Ann. Chim.* **1806**, *58*, 54–74.
25. Agmon, N. *Chem. Phys. Lett.* **1995**, *244*, 456–462.
26. Merinov, B. V. *Solid State Ionics* **1996**, *84*, 89–96.
27. Oza, A. *Cryst. Res. Technol.* **1984**, *19*, 697–707.
28. Bettinetti, G.; Novak, Cs.; Sorrenti, M. *J. Therm. Anal. Calorim.* **2002**, *68*, 517–529.
29. Nour, E. M.; Chen, L. H.; Laane, J. *J. Phys. Chem.* **1986**, *90*, 2841–2846.
30. Yu, X.; Houtman, C.; Atalla, R. H. *Carbohydr. Res.* **1996**, *292*, 129–141.
31. Yu, X.; Atalla, R. H. *Carbohydr. Res.* **2005**, *340*, 981–988.
32. Svensson, P. H.; Kloo, L. *J. Chem. Soc., Dalton Trans.* **2000**, 2449–2455.
33. Brock, C. P.; Morelan, G. L. *J. Phys. Chem.* **1986**, *90*, 5631–5640.
34. Dunitz, J. D.; Schomaker, V.; Trueblood, K. N. *J. Phys. Chem.* **1988**, *92*, 856–867.
35. Bürgi, H. B. *Annu. Rev. Phys. Chem.* **2000**, *51*, 275–296.
36. Peralta-Inga, Z.; Johnson, G. P.; Dowd, M. K.; Rendleman, J. A.; Stevens, E. D.; French, A. D. *Carbohydr. Res.* **2002**, *337*, 851–861.
37. Nimz, O.; Geßler, K.; Usón, I.; Laettig, S.; Welfle, H.; Sheldrick, G. M.; Saenger, W. *Carbohydr. Res.* **2003**, *338*, 977–986.
38. Kraus, W.; Nolze, G. *J. Appl. Crystallogr.* **1996**, *29*, 301–303.
39. Nolze, G.; Kraus, W. *Powder Diffr.* **1998**, *13*, 256–259.
40. Papaioannou, J. C.; Papadimitropoulos, N.; Mavridis, I. *Mol. Phys.* **1999**, *97*, 611–627.